PCCP

Accepted Manuscript

ROYAL SOCIETY OF CHEMISTRY

www.rsc.org/pccp

September 21, 2014

The Growth of Charged Platelets

C. Labbez[1], Bo Jönsson[2], Cliff Woodward[3], A. Nonat[1] and Maxime Delhorme[1,2]

[1)] *Laboratoire Interdisciplinaire Carnot de Bourgogne, UMR 6303 CNRS, Université de Bourgogne, 21078 Dijon Cedex, FRANCE*

[2)] *Theoretical Chemistry, Chemical Center, POB 124, S-221 00 Lund, SWEDEN*

[3)] *PEMS, University of New South Wales, Canberra, 260x ACT, AUSTRALIA*

Abstract

Growth models of charged nanoplatelets are investigated with Monte Carlo simulations and simple theory. In a first model, 2-dimensional simulations in the Canonical Ensemble are used to demonstrate that the growth of a single *weakly* charged platelet could be limited by its own internal repulsion. The short range attractive interaction in the crystal is modeled with a square well potential while the electrostatic interactions are described with a screened Coulomb potential. The qualitative behavior of this case can also be described by simply balancing the attractive crystal energy with the screened Coulomb repulsion between the crystal sites. This repulsion is a free energy term dominated by counterion entropy and of course reduced by added salt.

For a *strongly* coupled system, that is with high charge density and divalent counterions as in calcium silicate hydrate, the main product of cement hydration, the screened Coulomb approximation becomes inadequate and the growth behavior has to be described with the full primitive model. In this case, the energetic interactions become relatively more important and the entropy of the system plays a minor role. As a consequence, the electrostatic interactions gradually become less of a hindrance for aggregation and in extreme cases electrostatics actually promote the growth. This is manifested as an increased aggregation with, for example, increasing surface charge density.

In the presence of divalent calcium ions and at the high negative surface charge density typical for calcium silicate hydrate, electrostatic interactions are not a hindrance for an infinite growth of the particles. By combining experimental and simulated data we can show that the limited sized platelets found in cement paste is due to a very fast nucleation rate compared to the growth rate.

Introduction

Controlling the size of crystals and particles and more generally understanding the mechanisms affecting particle growth is of great importance for many applications - from building materials to advanced optical devices. The simple equilibrium picture is that once an aggregate has reach a certain size, the electrostatic repulsion will prevent further growth. Tolman [1] and later Overbeek [2] have proposed that the limited size of nanoparticles is an equilibrium result governed by electrostatics interactions. Recently, such a hypothesis was discussed by Jolivet et al. [3], who showed that the size of oxide nanoparticles could be tailored by precipitating the solid at varying pH values far from the point of zero charge, i.e. raising the surface charge at high enough values. Similarly, in protein solution it has been observed that the aggregation process halts once a certain aggregate size is reached. This has been explained as a result of internal Coulombic repulsion [4, 5, 6, 7], or if one prefers a lowered counterion entropy. Following the same idea, Schmit et al. [8, 9], using a model of charged particles with a short range attraction, described the competition between gel formation and meso-crystal formation as a result of differences in counterion entropy loss upon aggregation.

The situation in cement paste is qualitatively different with strong electrostatic interactions due to divalent calcium ions and a high surface charge density [10], which under *equilibrium* conditions might lead to an extended growth resulting in very large platelets. However, the conditions in early cement paste are far from equilibrium and a more likely scenario is one where the growth is *kinetically* controlled. During cement hydration, far from equilibrium, calcium silicate hydrate (C-S-H) nucleates onto the dissolving surface of tricalcium silicate grains, C_3S, [11] and the C-S-H platelets grow until they have reached a very limited size. The hydration proceeds as long as the supersaturation with respect to C-S-H is maintained (until C_3S is fully consumed) with a continuous germination and growth of new platelets next to the already existing ones forming a network. The network grows out into the solution [12, 13] and results in the setting and cohesion of the final material. The growth of C-S-H particles is both directional and limited and a typical C-S-H platelet has the approximate dimensions of $50 \cdot 30 \cdot 5$ nm [12, 14, 15].

In contrast to the nano sized platelets of C-S-H, giant, faceted and transparent single crystals of gypsum as long as 11 meters were recently found in Cueva de los Cristales, a cave in the Naica mine (Chihuahua, Mexico). It was shown that these crystals were formed under near-equilibrium conditions, maintained over a long period of time, ensuring an extremely slow nucleation rate, R_n and a slow growth rate, R_g. Based on classical nucleation and growth theory, Garcia-Ruiz et al. [16, 17], could show that the induction time, $t_{ind} \propto 1/R_n$, for the formation of gypsum nuclei was always above 1000 years. From the classical theory we obtain,

$$R_n \propto \exp\left(\frac{-16\pi\gamma^3 a^2}{3k^3T^3 \ln^2 S}\right) \tag{1}$$

where γ is the surface tension of the crystal, a the molecular volume, k the Boltzmann constant and T the absolute temperature. Indeed, as R_n depends on the supersaturation

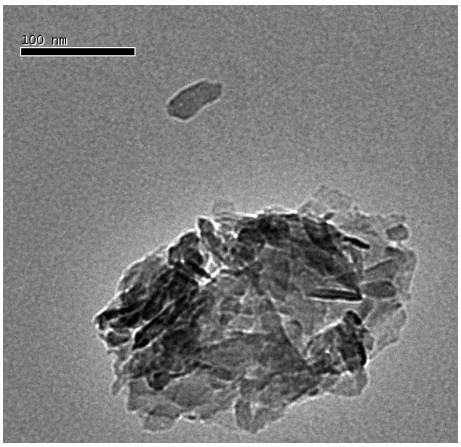

Figure 1: TEM image of C-S-H (x40 000) obtained from lime and silica. Platelets also aggregate. An isolated one shows the same size as in the case of C_3S hydration. The scale bar in the upper left corner is 100 nm. (From J. Haas, PhD Thesis, Nov. 2012, Universite de Bourgogne)

S, low values of R_n mean that supersaturation was kept very close to equilibrium during the crystallization in the cave.

On the contrary, the growth of particles at high supersaturation, far from equilibrium, is mostly a non-equilibrium process controlled by kinetics and the final outcome is a result from a competition between nucleation and growth. The growth rate, R_g, being defined as [16],

$$R_g \propto \exp(-\frac{A^{el} + A^{non-el}}{kT})(1 - \frac{1}{S}) \tag{2}$$

where A^{el} and A^{non-el} are the electrostatic and non-electrostatic components of the free energy barriers to the incorporation of molecules/atoms in the crystal lattice. Under such conditions, the resulting particles are most often small as a result of a fast nucleation rate compared to R_g, which consumes most of the feeding ions preventing particle growth. This is emphasized when the electrostatic barrier is high, see eq.(2), something to expect when the surface charge density of the nuclei/particles increases. With time, these particles often undergo changes of structure and morphology and finally grow in size, known as Ostwald ripening.

In ordinary cement paste (Portland cement), the supersaturation is controlled by the dissolution of C_3S and is typically on a high level, which means that the nucleation rate is high. At the same time, the surface charge density is very high possibly creating a significant free energy barrier slowing down the particle growth. Thus, both a large nucleation rate and a low growth rate act in the same direction resulting in nano sized C-S-H platelets. No long term growth has been observed in Portland cement. Nota bene, Portland cement has only existed for about 200 years! However, in a recent study of ancient Roman seawater concrete, obtained from the Pozzolanic reaction (i.e. mixture of lime and silica), micron sized C-S-H platelets were found [18].

An alternative to produce C-S-H particles is to grow them on a calcite surface at

high concentration of meta silicate and pH > 13, where initially small ordered particles are found on the surface. The ordering is probably facilitated by the calcite surface acting as a 2-dimensional template. When the concentratated silicate solution is replaced by various lime solutions at low degree of supersaturation, the C-S-H platelets partially recrystallize through Ostwald ripening and give rise to large particles. At low pH, i.e. low lime concentration, they can reach micron size, while at elevated pH, i.e. high lime concentration, smaller sub-micron sized particles are observed [19].

In this paper, we explore the growth of charged platelets in the weak and strong coupling regimes, that is weakly charged platelets neutralized by monovalent counterions and highly charged platelets neutralized by di- or multivalent counterions. A general result is that the screening by counterions and added salt is much stronger than predicted by mean field theory and, consequently, lead to particles with a larger equilibrium size than expected from this theory. In the really extreme cases with high electrostatic coupling, we even find that electrostatics promote aggregation! We discuss the results from both equilibrium and non-equilibrium perspectives in light of experimental observations on C-S-H.

Model Systems

Weakly charged platelet

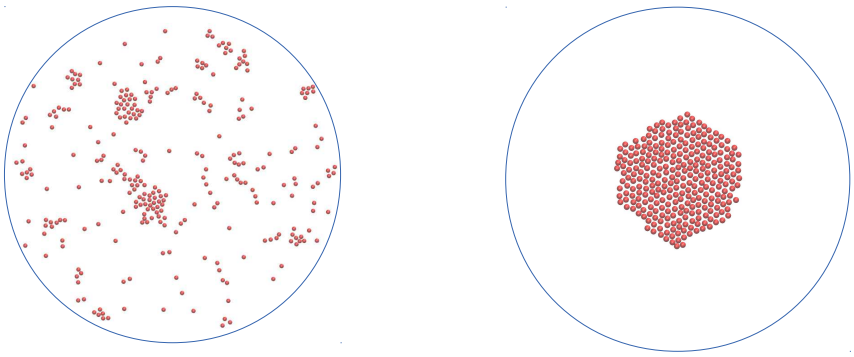

Figure 2: The final structures from two simulations with no electrostatic interactions and varying binding energy; $e_b = 2$ left graph and $e_b = 5$ right graph. $N = 289$ and $R_c = 378$ Å. A binding energy of $e_b = 2$ is not enough to maintain a compact cluster but $e_b = 5$ leads to an aggregated structure.

The model system depicted in Figure 2 is used to study the growth of a single platelet in two dimensions. Spherical particles, with radius $R = 5$ Å are allowed to move on a circular area with radius R_c. The interaction between any two particles i and j, with separation r_{ij} is given by a short-ranged square well potential, with depth e_b and width

w,

$$\begin{aligned} \beta u_{sw}(r_{ij}) &= \infty \quad r_{ij} < 2R \\ &= -e_b \quad 2R < r_{ij} < 2R + w \\ &= 0 \quad \text{otherwise} \end{aligned} \tag{3}$$

This potential has a generic attractive interaction that promotes aggregation, which we assume to be largely unaffected by other mobile ions. Crystals are likely held together via a combination of short-ranged electrostatic correlations, dispersion forces and covalent bonds. In addition, the particles that comprise the platelets experience strong electrostatic repulsion, which in a naive picture should counteract aggregation. This effect is modeled with a screened Coulomb potential, which also accounts for the ambient electrolyte concentration as well as counterion concentration,

$$\beta u_{sc}(r_{ij}) = \frac{l_B \exp(-\kappa r_{ij})}{r_{ij}} \quad r_{ij} > 2R \tag{4}$$

Here, $l_B = e^2/4\pi\epsilon_0\epsilon_r k_B T$ is the Bjerrum length, equal to 7.13 Å and κ is the inverse Debye-Hückel screening length, determined by salt and counterion concentration. The solvent (water) is treated as a dielectric continuum with a relative dielectric permittivity, $\epsilon_r = 78$. e is the elementary charge and ϵ_0 is the permittivity of vacuum. In the following we will quote all energies in units of kT.

Highly charged platelet

In the previous section with weakly charged platelets we approximated the presence of salt and counterions with a Debye-Hückel screening length and the crystal particles were confined to a plane. In this section all particles are allowed to move in three dimensions being confined to a spherical cell with radius, R_c, while the platelet can only form in an equatorial plane of 2 Å thickness. Thus, the square well potential is only acting between two crystal particles that happen to be within this layer. As in the single platelet model above, the solvent is treated implicitly using the primitive model. That is, charges are assumed to be embedded in a structureless dielectric continuum described by the relative dielectric permittivity and particles i and j interact via a Coulomb potential,

$$\beta u_{el}(r_{ij}) = \frac{l_B z_i z_j}{r_{ij}} \tag{5}$$

where z_i is the ionic valency of particle i and r_{ij} the particle separation. In this way, all mobile ions are treated explicitly, unlike the implicit treatment of salt and counterions used in the previous model. In addition to these electrostatic interactions we use the same attractive square well potential as before, eq.(3). The radius of the crystal particles was kept fixed at 5 Å unless otherwise mentioned and the radius of counter- and co-ions was 2 Å.

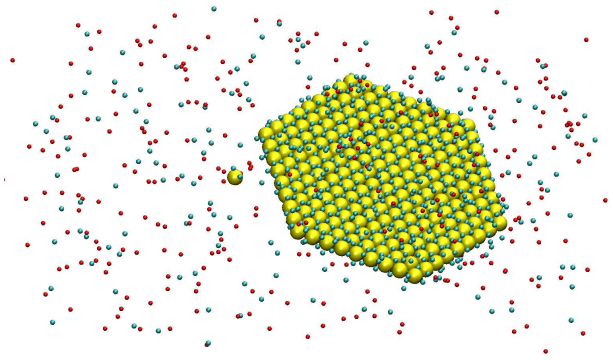

Figure 3: Simulation snapshot illustrating the setup used for force calculations between one crystal particle and the edge of a hexagonal platelet. The crystal particle is placed in the plane of the platelet. Small blue and red sphere represent the ions which are free to move within the cylindrical simulation cell, while the crystal particle and the platelet are maintained at fixed positions.

Most Monte Carlo simulations were carried out using the standard Metropolis algorithm in the canonical ensemble, i.e., constant number of particles, constant area/volume and temperature. A number of simulations were also performed with the grand canonical ensemble, where the salt chemical potential was maintained constant. These simulations were performed in a cylindrical cell with a frozen hexagonal platelet at its center and with co- and counterions moving freely within the cell. The size of the platelet, decorated by sites of varying charge Z_{site} arranged in a hexagonal pattern, see Figure 3, was varied. In these simulations the free energy cost to bring a crystal particle from the bulk solution to the edge of the platelet, $\beta A_{contact}$, was calculated. Note that $\beta A_{contact}$ is nothing but the electrostatic contribution to the free energy barrier to the growth. We have done so by placing an additional crystal particle in the plane of the platelet at different distances from the platelet center up to well defined lattice positions on the edge (referred as the *contact* point). The force acting on the crystal particle was calculated at each distance following the procedure described earlier [20]. The free energy of interaction between the crystal particle and the platelet was finally obtained by integrating the force. Note that in the following only the free energies at contact, referred as the electrostatic free energy barrier to the growth, are reported. In addition to the electrostatic interactions, all species were subjected to a strictly repulsive truncated and shifted Lennard-Jones potential U_{LJ}^{TrS}, instead of a hard core potential as above, to improve the force calculation statistics,

$$U_{LJ}^{TrS}(r_{ij}) = \begin{cases} \epsilon_{LJ}\left[\left(\frac{\sigma_{ij}}{r_{ij}}\right)^{12} - 2\left(\frac{\sigma_{ij}}{r_{ij}}\right)^{6}\right] + \epsilon_{LJ} & \text{if } r_{ij} < \sigma_{ij} \\ 0 & \text{otherwise.} \end{cases} \quad (6)$$

with $\epsilon_{LJ} = \mathrm{kT}$ and $\sigma_{ij} = (R_i + R_j)/2$ where R_i is the radius of species i.

Results

Weak coupling regime

We start with a simple analysis of the factors that control the growth of a single platelet. The free energy of the platelet is a combination of energetic and entropic contributions. The latter will disfavor aggregation, hence the energy term drives the clustering of particles and the formation of the platelets. It also provides a lower bound on the cluster free energy and hence an indication of its relative stability. That is, a stable cluster will always have a negative energy. We will use the words "cluster" and "platelet" as meaning the same thing, *i.e.* a collection of negatively charged (crystal) particles in the equatorial plane connected via the square well potential.

The cluster energy can be estimated from the potential model, eqs.(3) and (4). Assuming n particles in the cluster, the short-ranged binding energy is approximately $-nE_b$, where $E_b \approx me_b/2$ with m being the number of nearest neighbors. We assume that the range of the square well potential extends only to nearest neighbors. For the system we investigate, the most stable sphere packing in the plane is hexagonal, hence we choose m=6. The repulsive electrostatic energy can be estimated by integrating the screened Coulomb potential over the cluster area. We assume the latter to be circular, with radius $R_{clus} \approx \sqrt{n}R$.

$$E_{el} = \int_0^{R_{clus}} dr 2\pi r \frac{l_B}{\pi R^2} \frac{\exp(-\kappa r)}{r} = \frac{1}{l_{GC}} \int_0^{R_{clus}} dr \exp(-\kappa r) \tag{7}$$

where l_{GC} is the Gouy-Chapman length equal to $e/2\pi\sigma l_B$ with σ being the surface charge density of a platelet. This gives the following electrostatic energy per particle,

$$E_{el} = \frac{1}{\kappa l_{GC}}[1 - \exp(-\kappa R\sqrt{n})] = E_{el}^{\infty}[1 - \exp(-\kappa R\sqrt{n})] \tag{8}$$

where $E_{el}^{\infty} = 1/\kappa l_{GC}$ is the electrostatic energy (per particle) of an infinite cluster. This expression only approximately accounts for the truncating effects of the cluster boundary on the electrostatic potential. The total energy is thus

$$E_{tot} = n[(E_{el}^{\infty} - E_b) - E_{el}^{\infty} \exp(-\kappa R\sqrt{n})] \tag{9}$$

Minimizing with n, i.e., $\partial E_{tot}/\partial n = 0$, we obtain

$$\frac{(E_{el}^{\infty} - E_b)}{E_{el}^{\infty}} = (1 + \frac{\kappa R\sqrt{n}}{2}) \exp(-\kappa R\sqrt{n}) \tag{10}$$

If $E_{el}^{\infty} > E_b$, then eq.(10) has solutions corresponding to finite $n(> 0)$ and limited clusters can be stabilized. As $E_b \to E_{el}^{\infty}$ the cluster begins to grow uncontrollably, $n \to \infty$. Figure 4a gives the solution to eq.(10) for three different values of e_b. The dashed vertical lines, $\kappa = 1/3e_b l_{GC}$, shows the minimum value of κ for which the cluster growth is limited. That is, to the right of the dashed lines the crystal size is no longer electrostatically constrained

in size. Note, that this boundary is only determined by the binding energy and the Gouy-Chapman length. Simulations of this system were carried out in the Canonical Ensemble, so the conditions at which electrostatics does not constrain the cluster size are estimated as those where a single cluster forms in the simulation area. Clearly this estimate becomes more accurate in the thermodynamic limit. In Figure 4b we show the "phase diagram" derived from simulations of 222 particles in a circular simulation cell of radius 200 Å, together with the predictions based on our simple energy analysis. The theory gives a surprisingly good prediction of the boundary between finite and infinite clusters. The discrepancy at small binding energies can be explained by the neglect of the entropy.

Without any electrostatic interactions we observed from simulations that an initial single cluster disintegrates when $e_b \leq 2$. Increasing the binding energy to $e_b = 5$, one obtains a well-condensed single cluster. This cluster does not disintegrate upon introducing short-ranged electrostatic repulsions, $\kappa = 0.02$ Å^{-1}. However, for longer ranged repulsions, $\kappa = 0.015$ Å^{-1}, the single cluster breaks apart into smaller clusters. Figure 5 shows the distribution of cluster sizes in such a simulation - the clusters have a finite size and an average cluster consists of approximately 20 particles. Using eq.(10) we get $n \approx 13$. The agreement between simulations and the simple model is surprisingly good, considering the neglect of entropic and surface contributions to the free energy.

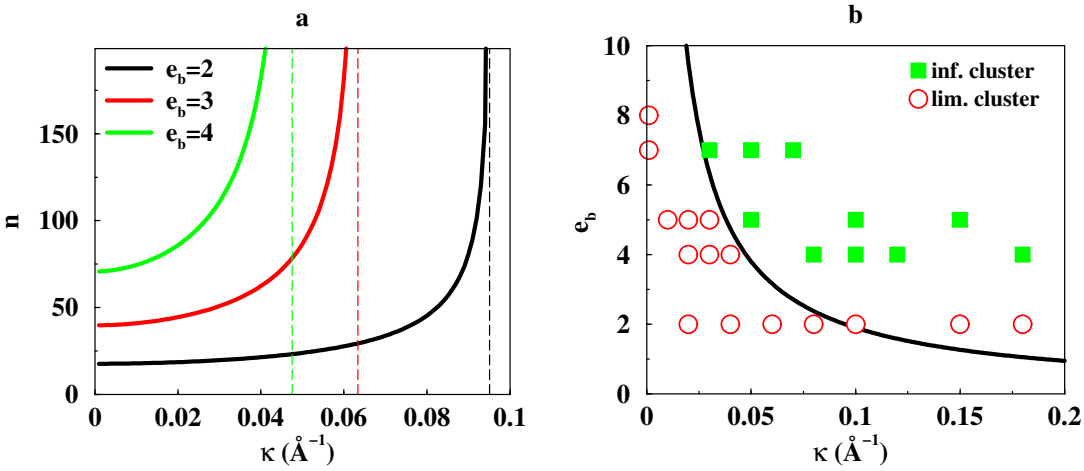

Figure 4: a) Solutions to eq.(10) for different binding energies as a function of electrostatic screening in terms of the Debye-Hückel inverse screening length. The dashed lines show the boundary at which the crystals start to grow infinitely. b) The black solid line shows the function $e_b = 1/\kappa l_{GC}$ describing the boundary between infinite and finite growth, from eq.(10). The symbols show the corresponding MC results obtained for a system with $N = 222$ and $R_c = 200$ Å.

Strong coupling regime

In this regime the simulations are carried out using the full primitive model where both crystal particles and counterions are explicitly described and are moving freely in a sphere. The size distribution of platelets is usually bimodal, see Figure 6. That is there is one(!)

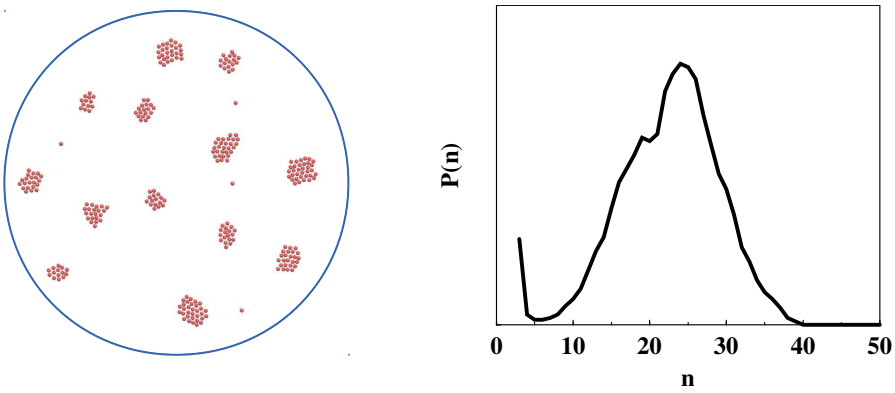

Figure 5: The final configuration from a simulation with $\kappa = 0.015$ Å^{-1}, $N = 289$, $R_c = 378$ Å and $e_b = 5$ - left graph - and the corresponding probability distribution for cluster size n.

large platelet and a few free "crystal particles". This means that a quantity like the average platelet size becomes less informative and we have instead calculated the average size of the largest platelet, $< N_{max} >$.

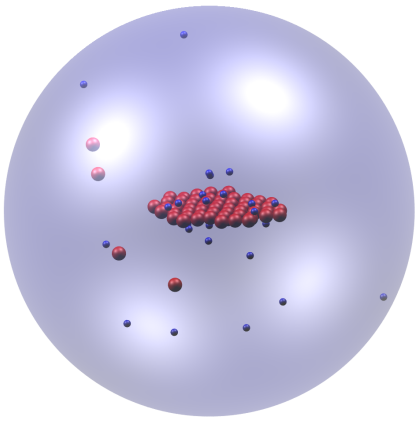

Figure 6: Snapshot from a MC simulation of 60 crystal particles (red spheres) and 30 divalent counterions (blue spheres). $R_c = 150$ Å and $e_b = 4$.

The importance of counterion entropy can be seen in Figure 7 where the cluster size is shown as a function of cell radius. When the cell radius increases, the platelet disintegrates and with $R_{cell} > 250$ the crystal has essentially disappeared. The concentration of divalent counterions with $N = 120$ and $R_c = 200$ Å is about 6 mM. One can note the qualitative difference between mono- and divalent counterions and that higher valency counterions promote the growth.

All simulations are performed within the Canonical Ensemble and in order to let the system grow we have to explicitly add particles. Figure 8 shows how the relative

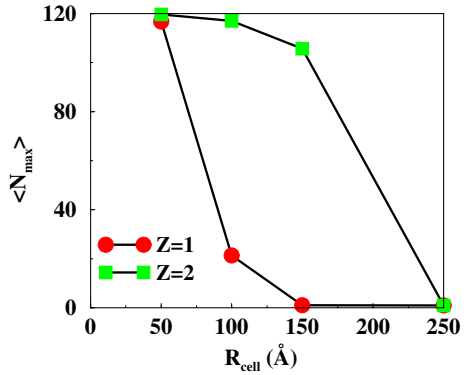

Figure 7: Average number of crystal particles in the largest cluster(=platelet) in a system with divalent counterions as a function of cell radius - $N = 120$, $e_b = 4$ and saltfree system.

cluster size, $< N_{max} > /N$, varies with number of crystal particles at constant density (3-dimensional), $3N/4\pi R_{cell}^3$. The variation is modest and one can note that the relative cluster size grows slowly with system size. One can once again note that the counterion entropy plays an important role, since with monovalent counterions there is no crystal growth. In same way, by reducing the surface charge density one can facilitate platelet growth. What we also find, in contradiction to the weakly coupled system studied with the screened Coulomb approximation, is that no finite sized platelets are formed. Either all particles aggregate and form the platelet or they completely disperse.

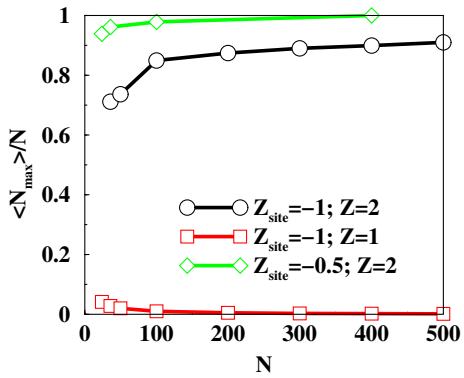

Figure 8: Fraction of crystal particles in the largest cluster(=platelet) as a function of number of crystal particles, N. Constant density, $e_b = 5$ and saltfree simulation.

Figure 9 shows the effect of increasing the surface charge density by increasing the crystal site charge while maintaining its size. This gives a formal area/unit charge ranging from 130 to 16 Å^2/e - the latter value being a bit too high expected for C-S-H. With divalent counterions we find a decreasing platelet size with increasing surface charge density and the platelets stop growing when $Z_{site} > 2$. By increasing the counterion valency to four, we find a qualitatively different behavior. Here the growth initially follows the divalent case, but for sufficiently high surface charge we see a positive slope, that is electrostatics promote aggregate formation.

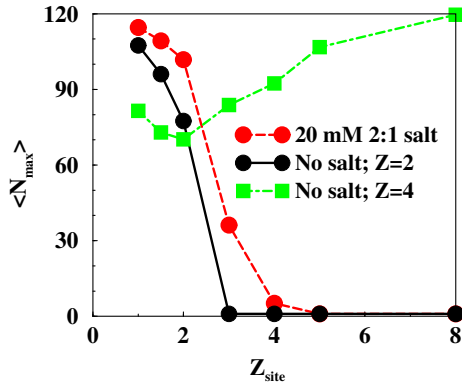

Figure 9: Number of crystal particles in the largest cluster(=platelet) as a function of crystal particles charge, Z_{site}. The number of crystal particles, $N = 120$. Black solid curve with filled circles: divalent counterions, $e_b = 5$, $R_c = 150$ Å and no salt; Red dashed curve with open circles: $Z = 2$, $e_b = 5$, $R_c = 150$ Å and 20 mM of 2:1 salt, green dot-dashed curve with open squares: $Z = 4$, $e_b = 4$ and R_c has been varied in order to maintain the same counterion concentration, no added salt.

Adding salt means that the simulations take a bit longer to converge and consequently the study has been limited in this respect. The salt effect is as expected - see Figure 9, that is the counterion entropy plays a smaller role and the cluster grows with increasing salt concentration.

Another way to study platelet growth, and in particular non-equilibrium effects, is by calculating the potential of mean force between a platelet and a crystal particle. We have done that for a cylindrical cell with a hexagonal platelet at its center and with co- and counterions moving freely within the cell. The results are shown in Figure 10 and 11. In Figure 10, the electrostatic free energy cost of adding a negatively charged crystal particle to the platelet edge is shown as a function of platelet size for divalent and monovalent counterions. The free energy cost reaches an asymptotic value for relatively small particle size for divalent counterions; but not for monovalent ones. In addition, much higher free energy barriers are found in the case of monovalent counterions, in good agreement with the growth simulations, Figures 7 and 8. Figure 11 shows how the electrostatic free energy barrier varies as a function of platelet charge density. The charge density is varied by maintaining a fixed particle size, $N = 127$, but increasing the negative charge of each site, Z_{site}. For sufficiently large counterion valency ($Z > 2$), the free energy has a non monotonic behavior similar to the curve shown in Figure 9.

Figure 11 shows how the electrostatic free energy at contact varies as a function of platelet charge density. The latter is varied by maintaining a fixed particle site, but increasing the negative charge of it. The same physical effects can also be found in Figures 8 and 9.

Discussion

In the case of a 1:1 salt, our simulations on the growth of platelets at the level of the screened Coulomb potential confirm the hypothesis first inferred by Tolam and Overbeek

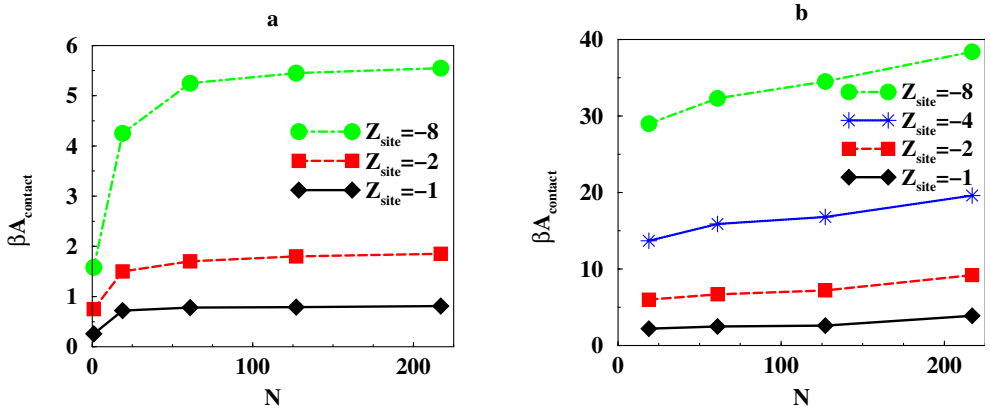

Figure 10: The free energy of interaction between a crystal particle and a hexagonal platelet of varying size at three different valencies of the crystal particle, Z_{site}. a) The counterions are divalent and the system is in equilibrium with a salt reservoir containing 20 mM of a 2:1 salt. b) The same as a) but with monovalent counterions and no salt. Note the different energy scale!

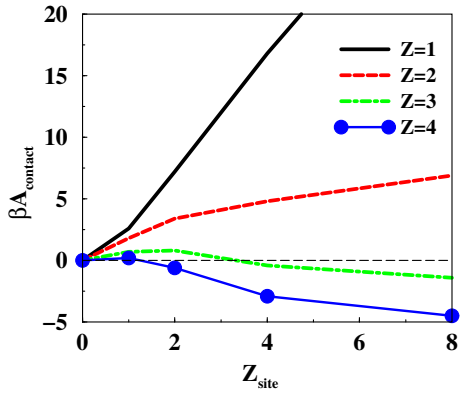

Figure 11: The free energy of interaction between a crystal particle and a hexagonal platelet (N=127) of varying charge density for four different valencies of the counterion in a saltfree system. The crystal particle is placed in a fixed site at the edge of the platelet.

and later observed experimentally on spherical particles[3], that electrostatics can stabilize particles at the nanometer scale. This can be seen in Figure 10b but maybe even better in Figure 11, where the free energy barrier for monovalent counterions is found to reach few tens of kT and to increase almost linearly with the platelet charge. Contrary to the divalent counterion case, we were not able to find a saturation in the free energy barrier while varying the particle charge, Z_{site}.

In the case of multivalent counterions, however, the picture is completely different. Indeed, already for divalent counterions the electrostatic free energy barrier to the growth is significantly reduced as compared to the case of monovalent counterions - see Figure 10 and 11. In salt free conditions, it is reduced from $\approx$ 15 kT to less than 5 kT when Z_{site} = 4. What is more, for $Z > 2$ and sufficiently large platelet charge densities βA^{el} is even found to become negative. In other words, in these latter cases electrostatics actually promote the growth - see Figure 11. These observations can be understood from the fact

that the importance of counterion entropy decreases with increasing valency - the number of particles is less.

A practical case of interest is the calcium-silicate-hydrate (C-S-H) found in cement. A particular puzzling question is why the hydrate particles are most often observed to be very limited in size? As already mentioned in the introduction, C-S-H nucleates and grows in supersaturated solutions rich in calcium most often around pH≈ 13. Under these conditions the C-S-H surface, which is covered with titrating silanol groups, reaches extremely high negative charge densities, of the order of 0.7 C/m^2[21]. Although high in absolute value, our simulations indicate that the electrostatic interactions alone can not stop the growth of C-S-H. Indeed, the corresponding free energy barriers to the growth are rather limited, at most not higher than ≈ 5 kT (see Figure 10) Even more so, when considering that usual binding energies for crystals typically are between 10 to 100 kT. This means that the nanometric C-S-H particles observed from hydration of C_3S, from the Pozzolanic reaction or from the reaction in sodium metasilicate/lime solutions do not have their true equilibrium size. Actually, micrometer sized C-S-H platelets were recently observed in 2000 years old Roman concrete [18], and have also been shown to grow on calcite monocrystal [22, 23]. We show below that these observations can consistently be explained within classical growth theory (CGT) and from the fact that nucleation is faster than the growth.

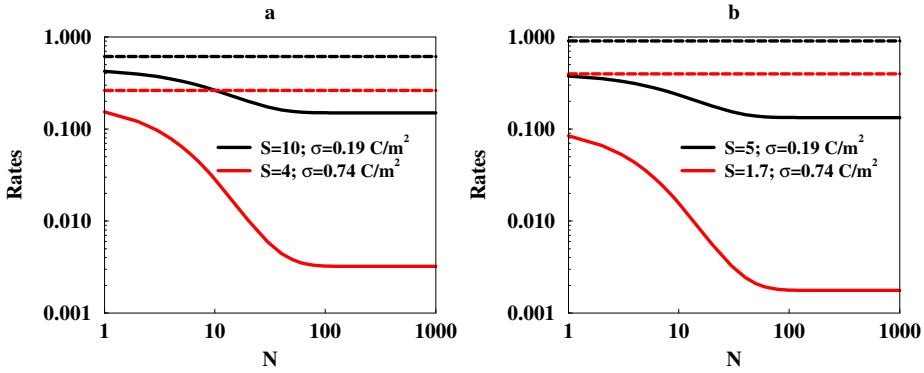

Figure 12: Initial rates of growth calculated from simulations (solid lines) and experimental nucleation rates(dashed lines) of C-S-H versus particle size at high and low surface charge densities (corresponding to high and low calcium hydroxide concentrations). A low calcium concentration corresponds to a low charge density, σ, and a high degree of supersaturation, S, and vice versa. The rates are presented as dimensionless quantities - see text for more details. a) In the case of heterogeneous nucleation on calcite and b) on C_2S.

Garrault et al. [11] have studied the nucleation of C-S-H and shown that the CGT is applicable. They measured the time to form the first nuclei and found the following homogeneous nucleation rate,

$$R_n \propto \exp(-\Delta A^*/kT) \approx \exp(-32/[\ln S]^2) \quad (11)$$

They also found that the free energy barrier, ΔA^*, for heterogeneous nucleation of C-S-H on calcite and on di-calcium-silicate, C_2S, is ten respectively one hundred times lower

than the corresponding free energy barrier for homogeneous nucleation. From these data and eq.(11) we can estimate the heterogeneous nucleation rates presented in Figure 12. The nucleation rate on tri-calcium-silicate, C_3S, is too fast to be accurately determined, indicating that ΔA^*_{C3S} is even lower than ΔA^*_{C2S}. Based on the simulated free energies we have calculated the growth rates for increasing (C-S-H) particle size for low and high lime concentration and compared to the experimentally determined rates of heterogeneous nucleation/growth on calcite and C_2S at the beginning of the hydration reaction, when the first C-S-H particles form (see Figure 12). For the calculation of the rates, the experimentally determined initial degrees of supersaturation [11], i.e. at the beginning of the C-S-H precipitation, were used. Note that the supersaturation degree depends on the reactive phase used (here calcite and C_2S)[11]. The simulated growth rates were determined from Eq.(2) using the electrostatic free energy barrier calculated from MC simulations, see Figure 10, with $Z_s = -2$ and $Z_s = -8$ for low and high $Ca(OH)_2$ concentrations, respectively. These site valencies are equivalent to negative charge densities of 0.19 and 0.74 C/m^2 in agreement with the experimental titration curve for C-S-H[21]. The non electrostatic free energy barrier to the growth is neglected and as a consequence, the growth rate is probably overestimated. Figure 12 shows that the growth rate, at the beginning of the hydration reaction, becomes rapidly negligible compared to the nucleation rate as the C-S-H platelets grow in size in response to the sharp increase of the electrostatic free energy with the particle size, see Figure 10. This is all the more true in the case of C_2S, Figure 12, and of C_3S, not shown, for which the nucleation rates are considerably higher.

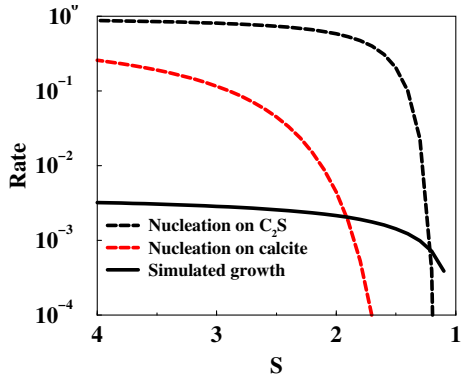

Figure 13: Nucleation and limiting growth rates of C-S-H versus degree of supersaturation, S, at high surface charge density (≈ at high $Ca(OH)_2$ concentrations) for heterogeneous nucleation and growth on calcite and C_2S. The rates are presented as dimensionless quantities - see text for more details.

As the hydration of C_2S and C_3S proceeds, the supersaturation decreases and reaches a constant value, corresponding to a steady state where the ions produced from the dissolution of the anhydrous phase are all consumed by the nucleation/growth of C-S-H. This continues until all the anhydrous phase is consumed. Figure 13 gives the variation of the limiting growth rate, for infinitely large platelets, and nucleation rate for C-S-H as a function of degree of supersaturation in the case of C_2S and calcite at high calcium hydroxide concentration. The limiting growth rate is obtained by extrapolating the free energy curves in Figure 10 to large particle sizes. In both cases, the nucleation rate is far

above the growth rate for a large range of supersaturation. In the case of C_2S, the crossing of rate curves occurs at a low degree of supersaturation, $S \approx 1.2$, below which the growth rate is very limited, < 0.0007. With C_3S it is even lower and with calcite the crossing takes place at $S \approx 1.9$, with the corresponding rate somewhat larger, ≈ 0.002, but still low enough to explain the very limited size of the C-S-H particles observed experimentally.

All these results show that the limited size often observed experimentally is not a thermodynamic stable state, but a consequence of both a relatively high nucleation rate and a (very) slow growth rate caused by the electrostatic contribution to the free energy barrier to the growth. The electrostatic interactions are, however, not strong enough to completely stop the growth.

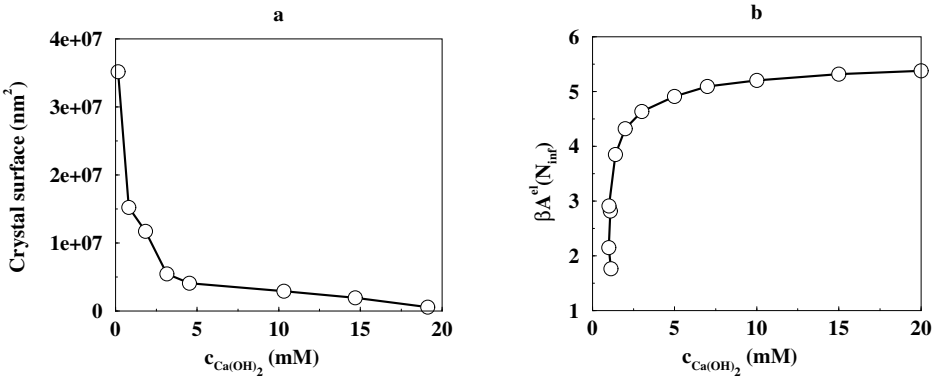

Figure 14: a) Surface area versus calcium hydroxide concentration for C-S-H particle grown by Oswald ripening on a calcite monocrystal. b) The corresponding simulated free energy barrier extrapolated to infinite particle size.

The contribution to C-S-H growth from electrostatic interactions is also illustrated in Figure 14a, which shows the size of C-S-H particles after one month of growth ("Ostwald ripening") on a calcite mono-crystal as a function of calcium hydroxide concentrations, that is increasing pH and absolute surface charge density. Figure 14b represents the variation of the calculated electrostatic free energy barrier for infinite platelet size versus the calcium hydroxide concentration. The latter was determined from an extrapolation of the free energy curves at the appropriate surface charge density determined experimentally from titration experiments of C-S-H[21]. The C-S-H surface area decreases rapidly when the calcium hydroxide concentration increases and the surface charge density of C-S-H increases in absolute value. Similarly, the electrostatic free energy barrier to the growth increases rapidly, or equivalently, the growth rate drops sharply, as the absolute surface charge density of C-S-H increases.

Conclusions

Charged platelets show different growth behavior depending on the strength of the electrostatic interactions. In a system with weakly charged platelets where the screened Coulomb approximation is applicable, it is always possible to find a (low) salt regime with limited

sized platelets, which of course will grow with addition of salt. Thus, there is an electrostatic free energy cost of growing the platelets. This free energy term is dominated by the counterion entropy. Platelet growth in the low coupling regime can also be illustrated with simple analytical arguments.

The surface charge density of C-S-H nanoplatelets in cement paste is very high and it is not possible to rely on simple mean field arguments, but we can still use the primitive model with explicit representation of all ions. In a real cement paste with a mixture of mono- and divalent ions the number of formal coupling parameters increases and we suggest to discuss in terms of energy and entropy dominated systems. The crystal growth will, for example, be facilitated if divalent counterions replace monovalent ones. In general, for parameters relevant for real cement systems our simulations predict an unlimited platelet growth in contradiction to experiments. Thus, we can conclude that the limited platelet size observed in cement paste is not an equilibrium phenomenon!

In order to investigate non-equilibrium aspects we have calculated the free energy cost of growth from the simulations. These free energies enable us to make qualitative statements about the nucleation and growth rates in cement paste. From a combination with experimental data, we can conclude that the limited growth of C-S-H platelets has a kinetic origin.

Acknowledgement: Financial support from the Region Bourgogne and computational support from CRI, Université de Bourgogne are gratefully acknowledged.

References

[1] R. C. Tolman, *J. Am. Chem. Soc.*, 1913, 35, 317.

[2] J.Th. G. Overbeek, *Far. Discuss. Chem. Soc.*, 1978, 65, 7.

[3] J.P. Jolivet, C. Froidefond, A. Pottier, C. Chaéac, S. Cassaignon, E. Tronc, and P. Euzen, *J. Mat. Chem.*, 2004, 14, 3281.

[4] W. C. Pan, O. Galkin, L. Filobelo, R. L. Nagel, and P. G. Vekilov, *Biophys. J.*, 2007, 92, 267.

[5] P. G. Vekilov, *Ann. N. Y. Acad. Sci.*, 2009, 1161, 377.

[6] B. Hutchens and Z. G. Wang, *J. Chem. Phys.*, 2007, 127, 084912.

[7] A. J. Archer, D. Pini, R. Evans, and L. Reatto, *J. Chem. Phys.*, 2007, 126, 014104.

[8] J. D. Schmit, S. Whitelam, and K. Dill, *J. Chem. Phys.*, 2011, 135, 085103.

[9] J. D. Schmit and K. Dill, *J. Am. Chem. Soc.*, 2012, 134, 3934.

[10] C. Labbez, B. Jönsson, I. Pochard, A. Nonat, and B. Cabane, *J. Phys. Chem. B*, 2006, 110, 9219.

[11] S. Garrault-Gauffinet and A. Nonat, *J. Cryst. Growth*, 1999, 200, 565.

[12] S. Garrault, E. Finot, E. Lesniewska, and A. Nonat, *C. R. Acad. Sci. Paris*, 1998, 327, 213.

[13] S. Garrault, E. Lesniewska, and A. Nonat, *Material and Structures*, 2005, 38, 435.

[14] D. D. Double, A. Hellawell, and S. J. Perry, *Proc. Roy. Soc. London. A*, 1978, 359, 435.

[15] A. Nonat, *Cement and Concrete Research*, 2004, 34, 1521.

[16] Y. Saito, *Statistical Physics of crystal Growth*, World Scientific, Singapore, 1996.

[17] J. M. Garcia-Ruiz, R. Villasuso, C. Ayora, A. Canals, and F. Otalora, *Geology*, 2006, 65, 327.

[18] M. D. Jackson, J. Moon, E. Gotti, R. Taylor, S. R. Chae, M. Kunz, A.-H. Emwas, C. Meral, P. Guttmann, P. Levitz, H.-R. Wenk, and P. J. M. Monteiro, *J. Am. Ceram. Soc.*, 96, 2598.

[19] A. Nonat, Unpublished data.

[20] M. Turesson, Bo Jönsson, and C. Labbez, *Langmuir*, 2012, 28, 4926.

[21] C. Labbez, I. Pochard, Bo Jönsson, and A. Nonat, *Cement and Concrete Research*, 2011, 41, 161.

[22] C. Plassard, E. Lesniewska, I. Pochard, and A. Nonat, *Ultramicroscopy*, 2004, 100, 331.

[23] C. Plassard, E. Lesniewska, I. Pochard, and A. Nonat, *Langmuir*, 2005, 21, 7263.